Constitutive Intracellular Na^+ Excess in Purkinje Cells Promotes Arrhythmogenesis at Lower Levels of Stress than Ventricular Myocytes from Mice with Catecholaminergic Polymorphic Ventricular Tachycardia

B. Cicero Willis, MD; MSc,[1] Sandeep V. Pandit, PhD;[1] Daniela Ponce-Balbuena, PhD;[1] Manuel Zarzoso, PhD;[1] Guadalupe Guerrero-Serna, PhD;[1] Bijay Limbu, MS;[2] Makarand Deo, PhD;[2] Emmanuel Camors,[3] PhD; Rafael J. Ramirez, PhD;[1] Sergey Mironov, PhD; [1] Todd J. Herron, PhD;[1] Héctor H. Valdivia, MD, PhD;[1] José Jalife, MD.[1,4]

[1]University of Michigan, Ann Arbor, MI; [2]Norfolk State University, Norfolk, Virginia, [3]University of Tennessee Health Science Center. [4]Fundación Centro Nacional de Investigaciones Cardiovasculares (CNIC), Madrid, Spain.

Online Supplement

Experimental Methods

Animals: The study was approved by the University Committee on the Use and Care of Animals at the University of Michigan and conforms to the Guide for the Care and Use of Laboratory Animals (NIH publication no. 85-23). Procedures for the generation of $RyR2^{R4496C+/-}$ CPVT mice[1, 2], $Cx40^{eGFP+/-}$ mice[3], and $RyR2^{R4496C+/Cx40eGFP}$ mice[1, 4, 5] are described elsewhere. $RyR2^{+/Cx40eGFP+/-}$ (hereafter Ctrl) and $RyR2^{R4496C+/Cx40eGFP}$ (hereafter CPVT) mice were used to enable visualization of the Purkinje network and isolated PCs via GFP expression (Supplemental Fig. S1). All mice were of either sex and 3-6 months old.[5]

Optical mapping: Littermate Ctrl and CPVT mice were used for optical mapping experiments. In Langendorff-perfused hearts, optical mapping of the subendocardium was conducted using fluorescent voltage (di-4-ANBDQPQ) and Ca^{2+} indicator (rhod-2 AM) dyes. High-resolution optical mapping was performed using a single 80x80-pixel CCD camera (Sci Measure, Decatur, GA, USA) and a custom-made LED system consisting of three lights for variable excitation of each wavelength of interest (blue for GFP; red for di-4-ANBDQPQ; green for rhod-2 AM).[6] For endocardial imaging and mapping, the right ventricular free wall was dissected from apex to base. Care was taken to ensure that coronary artery perfusion was undisturbed, while still allowing exposure of the septal and free-wall endocardium. GFP images were taken of the

mapping area to identify the PC network architecture and provide an anatomical frame of reference for subsequent analyses. Images were taken at the start and completion of each experiment to ensure the preparation had not moved; and that optical mapping recordings could be overlaid on the images.

Hearts were cannulated and perfused with normal Tyrode's solution containing (in mM) 130.0 NaCl, 1.0 $MgCl_2$, 1.2 NaH_2PO_4, 4.0 KCl, 1.8 Ca^{2+}, 5.6 glucose and 25.0 HEPES, pH 7.4, bubbled with 95% O_2 5% CO_2. Lead-I volume-conducted ECGs were acquired and digitized at 1 kHz (Axon Instruments MiniDigi 1A digitizer and AxoScope 10 software).[7] Optical mapping movies (4-6 s) were recorded throughout the duration of each experiment. The experimental protocol included 4 condition/recording groups: 1) baseline sinus rhythm; 2) high-frequency (12 Hz) pacing; 3) adrenergic stimulation (3.6 mM Ca^{2+}, 160 nM ISO); and 4) high-frequency pacing plus adrenergic stimulation. Once sinus rhythm stabilized, we recorded a baseline GFP image, as well as simultaneous membrane voltage (Vm) and Ca^{2+} movies. We then began right ventricular (RV) free wall point stimulation at 12 Hz for ≈5 sec. Movies from the last second of pacing and subsequent 5 sec of unpaced activity were recorded. Similar Ca^{2+} and voltage recordings were taken 5 min after a bolus injection of ISO (160 nM) in the presence or the absence of 3.6 mM extracellular Ca^{2+}. Analysis was performed using custom-made software.[2, 6]

Isolation of PCs and VMs: Mouse cardiac PCs and VMs were dissociated as previously described.[5, 8, 9] Mice were euthanized by CO_2 overdose. The heart was quickly excised, placed in cardioplegic solution containing (in mmol/L): glucose 280, KCl 13.44, $NaHCO_3$ 12.6, and mannitol 34. The aorta was cannulated and retrogradely perfused at 37°C for 4 min with a Ca^{2+}-free perfusion buffer containing (in mmol/L): 113 NaCl, 4.7 KCl, 1.2 $MgSO_4$, 0.6 Na_2HPO_4, 0.6 KH_2PO_4, 10 $KHCO_3$, 12 $NaHCO_3$, 10 HEPES, 10 2.3-butanedione monoxime (BDM, Sigma), 30 taurine, and 5.5 glucose bubbled with 100% O_2. For enzymatic digestion, collagenase type II (Worthington; 773.4 u/ml), trypsin (0.14 mg/ml), and $CaCl_2$ (12.5 µmol/L) were added to the perfusion buffer for ~5 min. Following digestion the ventricles were cut open and Purkinje fibers were extracted from the subendocardial surfaces. Cells were isolated by trituration of the tissue suspension in stopping buffer (perfusion buffer plus 10% fetal bovine serum and 12.5 µmol/L $CaCl_2$). At 37^o C, the Ca^{2+} concentration was gradually increased to 1.0 mmol/L with ~5 min incubation steps. Cells were spun at 1000 rpm and re-suspended in Tyrode's solution containing (in mM): NaCl 148, KCl 5.4, $MgCl_2$ 1.0, $CaCl_2$ 1.0, NaH_2PO_4 0.4, glucose 5.5, HEPES 15, pH 7.4 (NaOH). For permeabilized membrane experiments, cells were kept in Ca^{2+} free stopping buffer. Cells were used for electrophysiological recording within 4-6 hours after isolation.

PC and VM immunohistochemistry: Isolated cells were plated on laminin-coated glass coverslips, fixed with 4% paraformaldehyde (10 min), permeabilized with 0.1% Triton X-100, and washed with PBS. Endogenous mouse immunoglobulin was blocked using a mouse-on-mouse (anti-mouse Ig) blocking reagent (M.O.M. kit; Vector Laboratories, Burlingame, CA, USA) for 1 h at room temperature. Cells were further blocked for 1 h with 5% normal donkey serum in PBS (containing 0.1% Triton X-100), and subsequently incubated with primary antibodies overnight at 4°C. After washing,

donkey secondary antibodies (anti-mouse and anti-rabbit) conjugated to DyLight fluorophores (488, 549 nm; Jackson ImmunoResearch Laboratories, West Grove, PA, USA) were added for 1 h. Nuclei were stained with 100 µM 4′-6-diamidino-2-phenylindole (DAPI) and washed, and coverslips were mounted to microscope slides using ProLong Gold Anti-Fade Mounting Kit (Molecular Probes, Eugene, OR, USA). Immunofluorescence was examined with a Nikon Eclipse Ti inverted confocal microscope with a ×63/1.2-NA oil objective (Nikon Inc., Tokyo, Japan) at ambient temperature. Rabbit anti-$Ca_V1.2$ (Alomone, Jerusalem, Israel) and mouse anti-RyR2 (Iowa Hybridoma Core, University of Iowa) antibodies were used.

Simultaneous action potential (AP) and Ca^{2+} transient measurements: APs were recorded with a MultiClamp 700B amplifier coupled to a Digidata 1440A digitizer (Molecular Devices). Isolated cells were patched using 2-3 MΩ borosilicate glass pipettes filled with intracellular solution containing (in mM): KCl 140.0, MgCl2 1.0, MgATP 7.0, NaGTP 0.3, HEPES 10.0 (pH 7.2 adjusted with KOH) with 100µM fluo-4 pentapotassium salt (Life Technologies). Isolated cells were placed on laminin coated corverslips and perfused with heated (37°C) Tyrode's solution. Ca^{2+} signals were recorded using a whole-cell fluorescence photometry acquisition system (IonOptix), with a 485±5 nm excitation light source emission filter and a 500-550 nm acquisition band pass filter. Fluorescent signals were synchronized to AP recordings via a TTL connection between systems. Single isolated VMs or PCs were selected within the fluorescence detection window, then gigaohm seal patch-clamped in the whole-cell configuration. Fluorescence gain and offset were appropriately adjusted. Cells were stimulated at increasing frequencies (1, 3, 5 Hz) by current injection via patch-pipette using a DS-8000 digital stimulator (World Precision Instruments) at twice threshold. Steady state and post-pacing baseline activities were recorded in all cells. Fluorescence analysis was performed using IonOptix software.

Ca^{2+} transients and Ca^{2+} sparks: Measurements were acquired with a Nikon A1R confocal microscope in line scan mode on a 12-bit (4096 grayscale) acquisition system. Pixel size was adjusted to 150 nm, pinhole aperture was 1.2 Airy units, and acquisition frequency was 512 Hz. Isolated cells were incubated for 30 min in normal Tyrode's solution containing 10 µM rhod-2 AM, then washed with a fluorophore-free solution and de-esterified for 15 min. Cells were placed on laminin-coated glass coverslips, mounted in a temperature-controlled superfusion chamber (37°C) and perfused with Tyrode's solution. Lines scans were parallel to the longitudinal axis of cells, avoiding cell nuclei. For Ca^{2+} transients, Ctrl and CPVT VMs and PCs were field-stimulated at incrementing pacing frequencies (1, 3, and 5 Hz) to reach steady-state SR Ca^{2+} load. The last paced event was recorded along with the subsequent 2-3 s for spontaneous Ca^{2+} spark recordings. The protocol was repeated at 1 Hz after 5 and 10 min of 10 nM ISO perfusion. Fluorescence data were normalized as $\Delta F/F_0$, where F is fluorescence intensity and F_0 is the average fluorescence at rest. For Ca^{2+} spark analysis, a 2-s line scan image window was selected 3 s after a steady-state Ca^{2+} transient had decreased to baseline level. Cells that developed Ca^{2+} waves within this time period were excluded from analysis. Ca^{2+} spark analysis was performed using ImageJ (National Institutes of Health).[10, 11]

Permeabilized cellular Ca^{2+} spark recordings: Isolated VM and PCs were perfused with 50nM free Ca^{2+} internal solution containing: (in mM): EGTA 0.5, HEPES 10, K-aspartate 120, $MgCl_2$ 0.56, $CaCl_2$ 0.12, ATP-Mg 5, reduced glutathione 10, phosphocreatine di-Na 5, creatine phosphokinase 5U/ml, dextran 4% plus saponin 0.005% for 1 min for membrane permeabilization, then perfused for 5 min with internal solution containing 2.5 μM fluo-4 penta-K^+ (LifeTechnologies). Confocal line scan recordings (4-s duration) were obtained and analyzed within 10 min after dye loading as described above.

SR Ca^{2+} load: Experiments were performed using the whole-cell fluorescence photometry acquisition system (IonOptix). Cells were loaded with rhod-2 (Life Technologies) as described above. Cells were placed on laminin-coated coverslips and perfused with heated (37°C) Tyrode's solution containing 1 mM Ca^{2+}. Single cells were electrically paced at 3Hz for 10 seconds to reach steady-state SR Ca^{2+} load. 100 ms after pacing, the cell was quickly perfused with Tyrode's solution containing caffeine (10mM). SR Ca^{2+} load was calculated from the $\Delta F/F_0$ of the cytosolic Ca^{2+} signal evoked by caffeine application. Steady-state Ca^{2+} transient amplitude was presented as a fraction of the caffeine induced Ca^{2+} transient amplitude. Time to 50% decay was estimated from time at maximal caffeine induced Ca^{2+} transient amplitude.

Na^+/Ca^{2+} exchange current (I_{NCX}): Whole cell patch-clamp recordings were performed using borosilicate glass pipettes (1.8-2.4 MΩ). Cells were perfused with external solution containing (in mM): 130 NaCl, 1.2 $MgSO_4$, 1.2 NaH_2PO_4, 1.8 $CaCl_2$, 10 HEPES, and 10 glucose (pH 7.4 with CsOH). Nifedipine (10 μM), ouabain (1 mM), and niflumic acid (10 μM) were added to block L-type Ca^{2+}, Na^+/K^+-ATPase and Cl^- currents, respectively. Pipette solution contained (in mM) 100 Cs^+-glutamate, 7.25 Na^+-HEPES, 1 $MgCl_2$, 12.75 HEPES, 2.5 Na_2ATP, 10 EGTA, and 6 $CaCl_2$ (pH 7.2 with CsOH). Free Ca^{2+} in pipette solution was 205 nM, calculated with dissociation constants given in MaxChelator software. Current was elicited using a descending-ascending voltage ramp (from +100 to -120 and back) from a holding potential of -75 mV. I_{NCX} density was determined as the $NiCl_2$ (1mM)-sensitive current, which was subtracted from baseline recordings and normalized to cell capacitance.

Intracellular Na^+ measurements ($[Na]_i$): Experiments were recorded and analyzed using a fluorescence photometry acquisition system (IonOptix). Briefly, isolated cells were incubated in Tyrode's solution containing 5μM SBFI-AM (Life Technologies) and 0.05% Pluronic F-127 for 2 hours, followed by 30 min in Tyrode's solution for desterification. Cells were plated in laminin-coated coverslips and perfused with warm (37°C) Tyrode's solution. Dual excitation (340 and 380 nm) was performed in each selected cell at rest and under 2Hz pacing (5 min). After pacing, each cell was perfused with divalent-free solution containing strophantidin (100μM) and gramicidin (10μM) and increasing free Na^+ concentrations (5, 10 and 20 mM Na^+, respectively), as previously described.[12] Background-subtracted F_{340}/F_{380} ratio was then converted to $[Na^+]_i$ by using a three-point calibration at the end of each experiment.

Biophysical numerical model of murine Purkinje cell: A morphologically realistic biophysical model of a murine cardiac Purkinje cell (PC) was developed starting from

the model of Vaidyanathan et al.[9] Figure S2 shows a schematic of the PC model. The cell is assumed to be cylindrical in shape with 129 µm length and 8 µm width which is within the experimentally measured dimensions of 129±7 µm and 8±0.3 µm, respectively.[9] Fig. S2B shows the intracellular compartmentalization of the model which is assumed to be symmetric along the length. The sarcolemmal (SL) currents are uniformly distributed along the length and the SR is assumed to be in the core of the cell. The membrane currents are collected in a subSL region of 0.5 µm depth immediately below the SL. The SR consists of two compartments: 1) a release compartment called Junctional SR (JSR) which is responsible for the release of Ca^{2+} from SR into the cytosol (blue arrow), and 2) an uptake compartment called Network SR (NSR) which is responsible for the uptake of Ca^{2+} from the cytosol into the SR (red arrow). Similar to SL, the ionic fluxes to and from the SR are collected in a sub-sarcoplasmic reticulum (subSR) region of 0.5 µm depth surrounding the SR. The radius of the SR is 4 µm and the total width of the cytosolic region is 2 µm surrounding the SR. The ionic formulations of the model were based on the work done by Li et al.[13] and modified according to the experimental data.[9] The ionic model described in [9] was modified to include late sodium current (I_{NaL}) as described in later section.

Cytosolic Ca^{2+} diffusion process: A realistic two component cytosolic Ca^{2+} diffusion process, as observed experimentally[14] was implemented in our model as follows: 1) Radial diffusion of Ca^{2+} entering the cell via SL Ca^{2+} channels (I_{CaL} and I_{CaT}) propagating towards central core (SR), referred to as wavelets, and 2) Cell wide longitudinal Ca^{2+} diffusion wave (CWW) initiated as a result of local CICRs propagating along the length of the cell. The length of the cell was divided into 10 discrete discs with each disc possessing L- and T-type SL Ca^{2+} channels and a SR compartment, whereas the width of the cell was divided into 81 concentric layers as shown in Fig. S3. The discretization of the cell volume was necessary to implement the uniform longitudinal and radial Ca^{2+} diffusion process. The number of SR discs was constrained to 10 to minimize the computational load while maintaining adequate spatiotemporal Ca^{2+} resolution.

A three dimensional diffusion equation was used to model the cytosolic Ca^{2+} diffusion process as follows:[15, 16]

$$\frac{\partial c}{\partial t} = \beta_i(c).[D_{Car}\frac{\partial^2 c}{\partial r^2} + \frac{D_{Car}}{r}\frac{\partial c}{\partial r} + D_{Cal}\frac{\partial^2 c}{\partial x^2} + J_{Ca}] \quad (1)$$

where c is the intracellular Ca^{2+} concentration, $D_{Car}\frac{\partial^2 c}{\partial r^2} + \frac{D_{Car}}{r}\frac{\partial c}{\partial r}$ term represents the radial diffusion and $D_{Cal}\frac{\partial^2 c}{\partial x^2}$ represents longitudinal diffusion. Here, D_{Cal} and D_{Car} represent the longitudinal and radial diffusion coefficients, respectively. J_{Ca} is the radially propagating Ca^{2+} flux from the SL channels and the ryanodine receptor flux from the SR and $\beta_i(c)$ represents the Ca^{2+} buffers. Finite Difference Time Domain (FDTD) solution[17] was used to a produce a finite and linear equivalent of Equation 1 as:

$$c_{(n,k,t)} = \beta_i(c_{(n,k,t)}) \frac{D_{Car}}{j_n(\Delta r)^2}[(1+j_n)c_{(n+1,k,t)} - 2j_n c_{(n,k,t)} + (j_n - 1)c_{(n-1,k,t)}] + \left\{ \frac{D_{Cal}}{(\Delta x)^2}[c_{(n,k+1,t)} - 2c_{(n,k,t)} + c_{(n,k-1,t)}] \right\} \quad (2)$$

Where $c_{(n,k,t)}$ represents intracellular Ca^{2+} concentration at a discrete node (n,k) at a time instance t. Here *n* represents the number of rows used in the model, *k* represents the number of columns used in the model, *Δr* is a small increment in width of model, *Δz* is a small increment in the length of the model, and j_n represents the n^{th} row along radial axis of cylindrical model. The value of the diffusion coefficient ($D_{Cal} = D_{Car} = D_{Ca}$) in our model was chosen to be 7 μm²/ms to reproduce experimentally observed Ca^{2+} transients. The Ca^{2+} transients obtained in our model are compared with the experimentally recorded values in Table S1.

Late sodium current (I_{NaL}): I_{NaL} formulation described in Li and Rudy[18] was included in the PC model. It included two components, namely, $I_{NaL,2}$ which peaks at -20 mV and $I_{NaL,3}$ which activates in the pacemaker range (see Equation 3

$$I_{NaL,2} = \overline{G}_{NaL,2} \cdot m_{L2} \cdot h_{L2} \cdot j_{L2} \cdot (V - E_{Na})$$
$$I_{NaL,3} = \overline{G}_{NaL,3} \cdot m_{L3} \cdot h_{L3} \cdot j_{L3} \cdot (V - E_{Na}) \quad (3)$$
$$I_{NaL} = I_{NaL,2} + I_{NaL,3}$$

where $\overline{G}_{NaL,x}$, m_{Lx}, h_{Lx}, and j_{Lx} are the maximum conductance, activation gate, fast inactivation gate, and slow inactivation gate of $I_{NaL,x}$ current, respectively. Further details about the gating parameters and initial conditions can be found in Ref. [9] The peak current density was adjusted to 1 pA/pF based on the experimental data reported by Iyer et al.[19] in mouse PCs.

The model was paced at 1 Hz for 5 mins to attain the steady state values. Table S2 provides a comparison of AP parameters obtained in our model with those of Vaidyanathan et al.[9] Fig. S3 shows the AP morphology of our model compared to the experimentally recoded AP.[9] Intracellular sodium concentration ($[Na^+]_i$) was increased by systematically reducing the sodium potassium pump current (I_{NaK}) as given in Table S3. Elevated $[Na^+]_i$ levels led to increase in the averaged intracellular Ca^{2+} in PC model as listed in Table S5.

Supplemental Tables

Table S1. The parameters of average calcium transients recorded in the experiments[1] and those obtained in the model.

Parameter	Experiments	Model
Peak Amplitude	31.193 ± 0.91 AU	1.03 µM
Time to Peak	18.8 ± 13.2 ms	27 ms
Decay time	261 ± 69.18 ms	199 ms

Table S2. Comparison of the AP parameters recorded in experiments[1] with those obtained in the model.

Parameter	Experiments	Model
dV/dtmax (mV/ms)	212±15	211.37
APD_{50} (ms)	4.7±0.3	7.7
APD_{70} (ms)	14.4±1.6	15.5
APD_{90} (ms)	68.6±5	67.1

Table S3. Intracellular sodium concentrations obtained for different scaling of I_{NaK}.

I_{NaK} scaling (%)	$[Na^+]_i$ (mM)
100 (Control)	12.42
85	13.57
75	14.58
65	15.91

Table S4. Modifications to the PC model for implementing the functional effects of isoproterenol.

Ionic Currents	Modification in percentage
I_{CaT}	230 %
I_{CaL}	140 %
I_{NaK}	170 %
I_{K1}	80 %

Table S5. Intracellular averaged calcium concentrations for different scaling of I_{NaK}.

I_{NaK} (%)	Peak Average $[Ca^{2+}]i$ (μM)
100 (Control)	1.03
85	1.28
75	1.49
65	1.81

Table S6. Resting membrane potentials and corresponding values of fast and slow inactivation gates (*h* and *j*, respectively) of I_{Na} at various elevated levels of $[Na]_i$.

I_{NaK} (%)	V_m (mV)	*h*	*j*
100 (Control)	-73.8	0.8384	0.8598
85	-73.6	0.8329	0.8541
75	-73.45	0.8282	0.8492
65	-73.27	0.8217	0.8423

Table S7. Action Potential characteristics in the PC model with and without I_{NaL}

I_{NaK} (%)	dV/dtmax (mV/ms)		Vrest (mV)		APD_{90} (ms)	
	With I_{NaL}	Without I_{NaL}	With I_{NaL}	Without I_{NaL}	With I_{NaL}	Without I_{NaL}
100 (Control)	211.37	212.2	-73.8	-73.95	67.1	51.4
85	206.72	207.73	-73.6	-73.75	78.3	59.9
75	202.73	203.9	-73.45	-73.65	85.4	64.8
65	197.54	199.05	-73.27	-73.45	95.5	71.5

Supplemental Figures

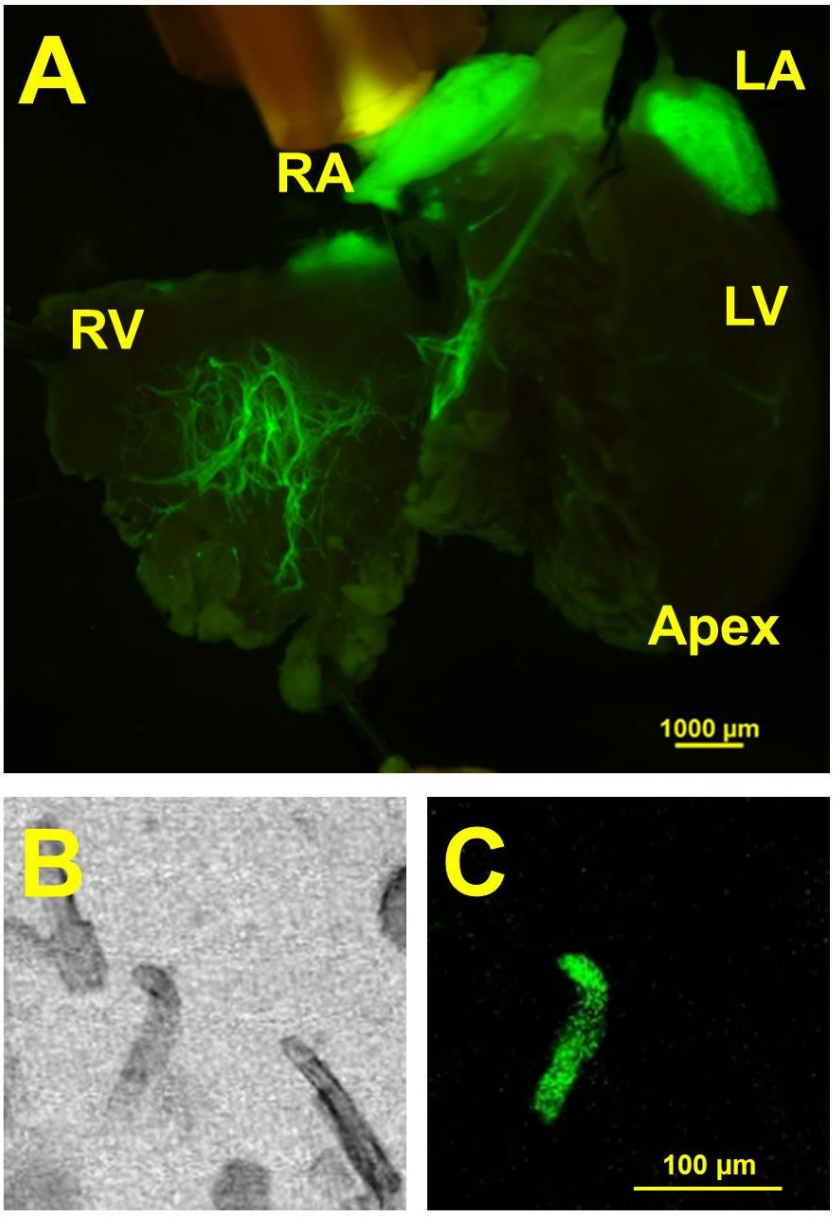

Supplement Fig. S1. Fluorescence of Cx40$^{eGFP+/-}$ mice endocardial Purkinje fibers and isolated PCs. (A) GFP fluorescence image of Cx40$^{eGFP+/-}$ CPVT heart RV endocardial preparation. (B) Light-transmitted and (C) fluorescence image of isolated GFP positive PC. LA= left atrium. LV= left ventricle. RA= right atrium. RV= right ventricle.

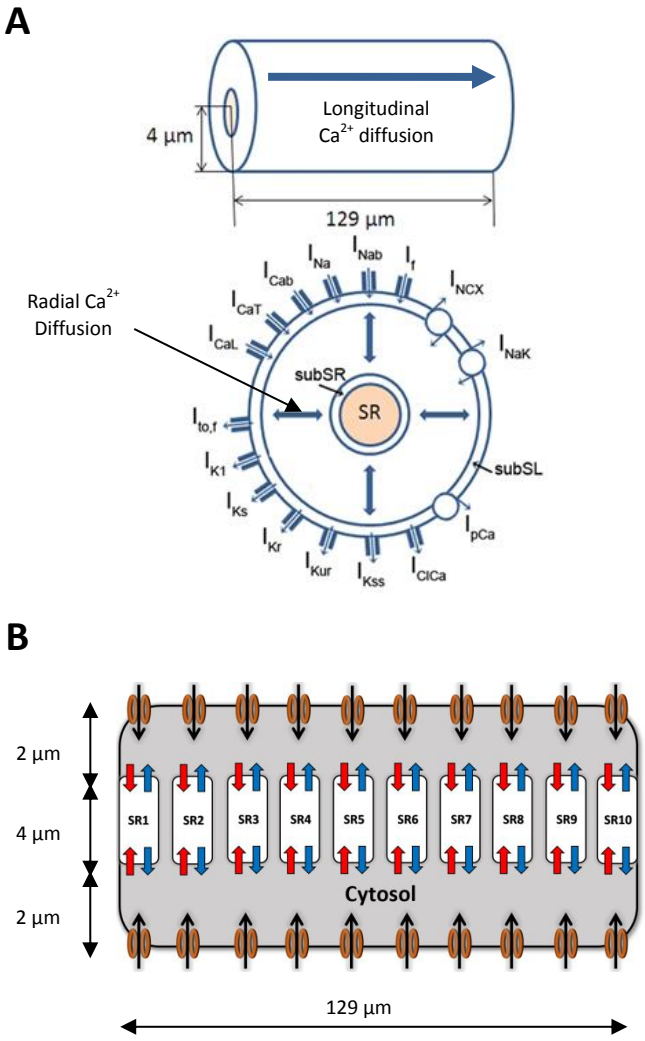

Supplemental Fig. S2. (A) Schematic showing various ionic currents and two components of Ca^{2+} diffusion (radial and longitudinal) in the PC biophysical model. (B) The sarcoplasmic reticulum (SR) is divided into 10 discrete sub compartments (SR1-SR10) along the cell length each having its own Ca^{2+} release/uptake machinery.

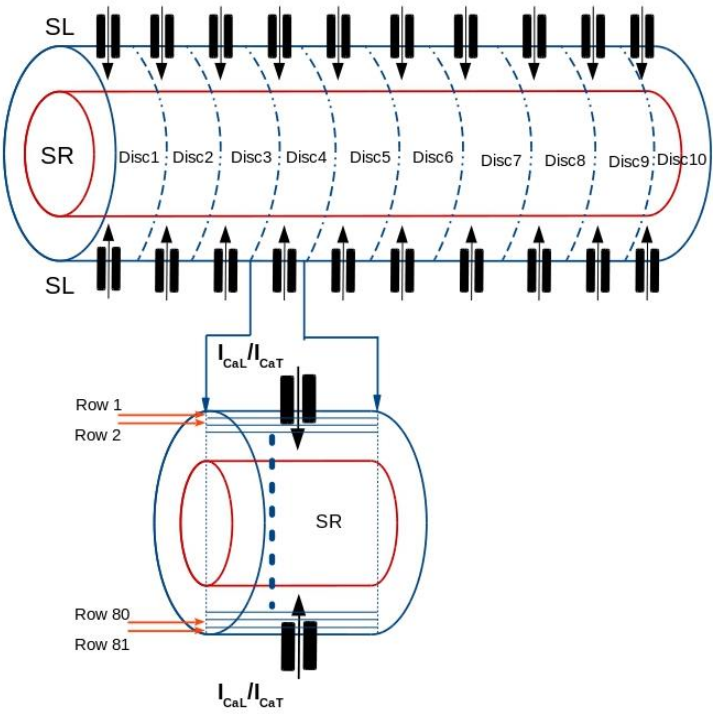

Supplemental Fig. S3. Implementation of spatio-temporal diffusion in the PC model. The Cell is divided into 10 Discs, each consisting of 81 concentric layers (rows).

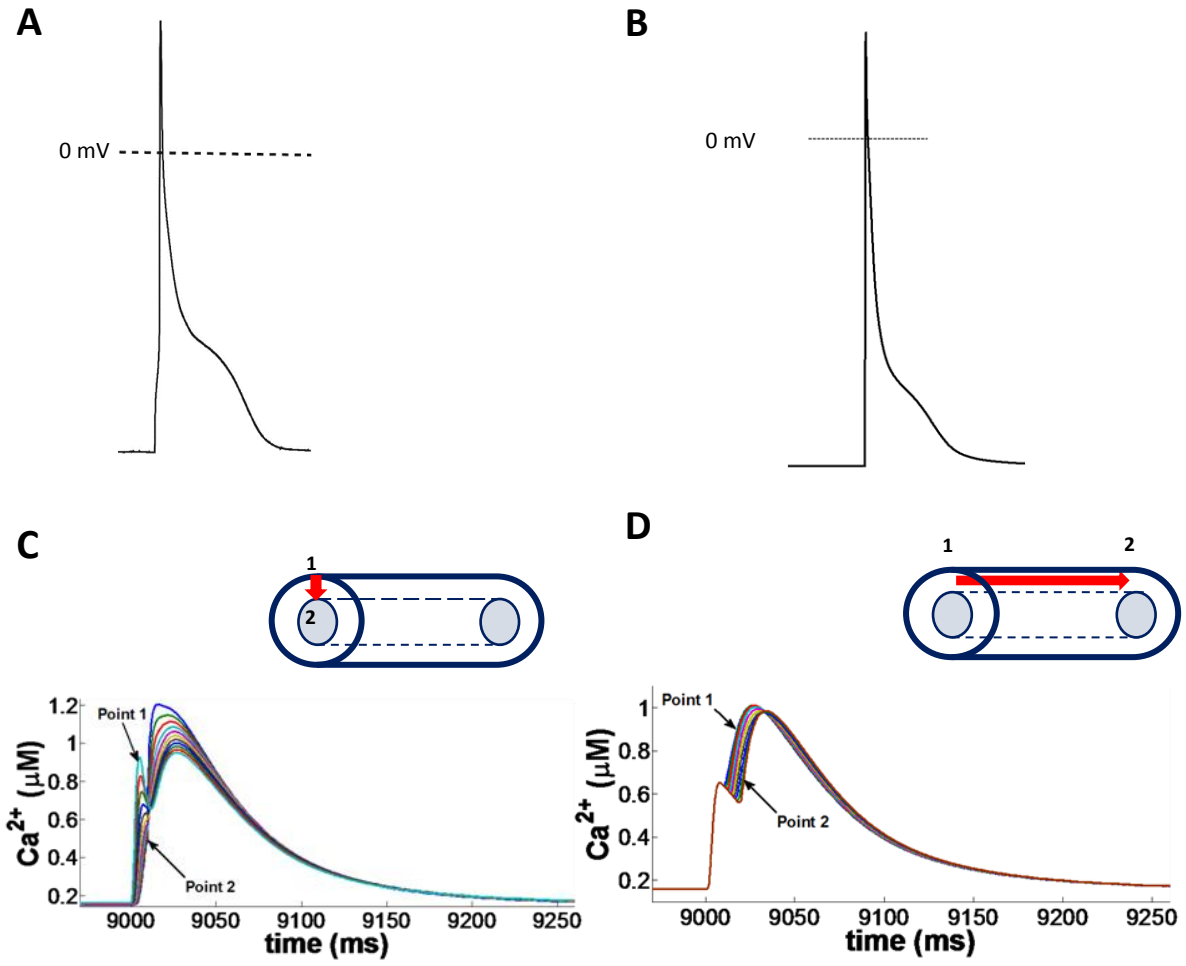

Supplemental Fig. S4. AP morphology (A) as experimentally recorded in mouse PCs by Vaidyanathan et al.,[9] (B) AP obtained from our PC model. Cytosolic Ca^{2+} transients observed in the model representing (A) diffusion of radial wavelets, and (B) longitudinal diffusion of CWW. The locations of Point 1 and Point 2 are shown on the right. The red arrow represents the component of Ca^{2+} diffusion shown.

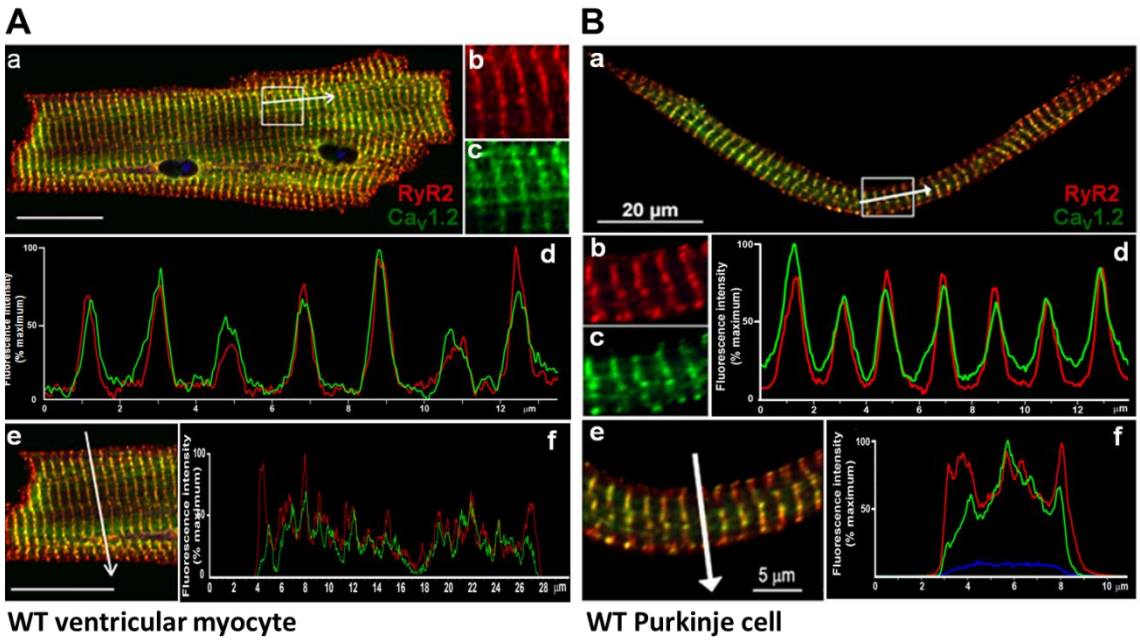

Supplemental Fig. S5. Subcellular co-localization of RyR2 and $Ca_V1.2$ is more heterogeneous in Ctrl PCs than VMs. (A) Ventricular myocyte, (B) Purkinje cell. For each Panel, subpanels (b-c) are enlarged regions of the boxed area in (a). Co-localization RyR2 and $Ca_V1.2$ is shown in (b-d) at the T-tubules and at the sarcolemma (e-f). Red, RyR2; Green $Ca_V1.2$.

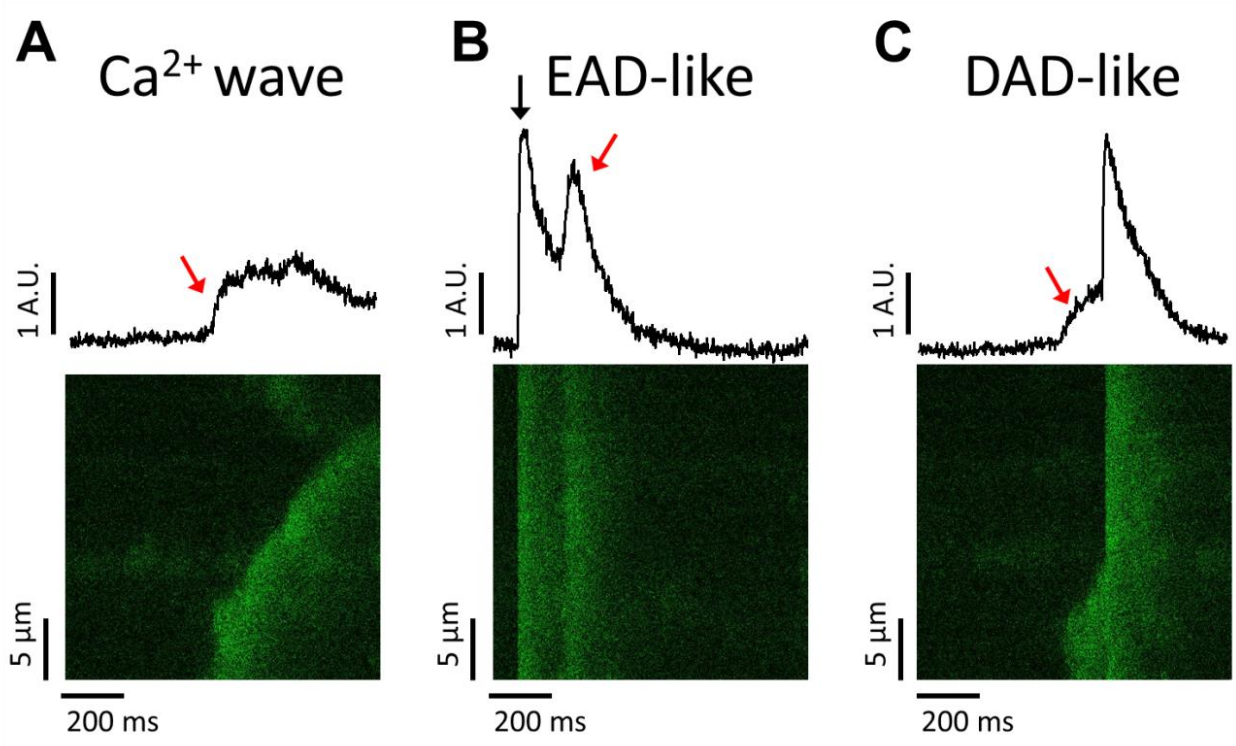

Supplement Fig. S6. Representative examples of spontaneous Ca^{2+} release in CPVT PCs perfused with 30nM Isoproterenol. Left is a diastolic Ca^{2+} wave. Middle shows an early after Ca^{2+} transient after a paced Ca^{2+} transient. Right illustrates a diastolic Ca^{2+} wave that leads to triggered activity (delayed after Ca^{2+} transient). All of these are present in both Ctrl and CPVT Purkinje cells. Black arrow marks paced beat, red arrow indicates spontaneous Ca^{2+} event.

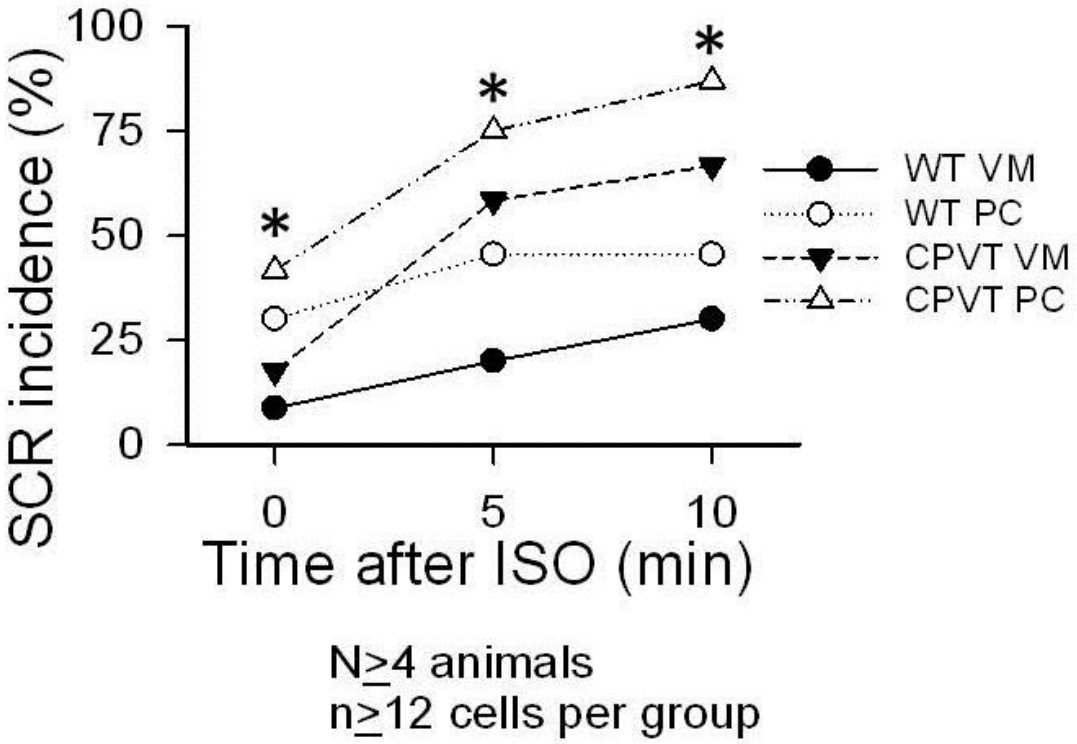

Supplement Fig. S7. Increased spontaneous Ca^{2+} release incidence in CPVT PCs. The incidence of spontaneous Ca^{2+} release increases with perfusion of 10nM isoproterenol. The incidence of SCR is higher in CPVT PCs both baseline and after ISO. *$p<0.05$ using Fisher's exact test.

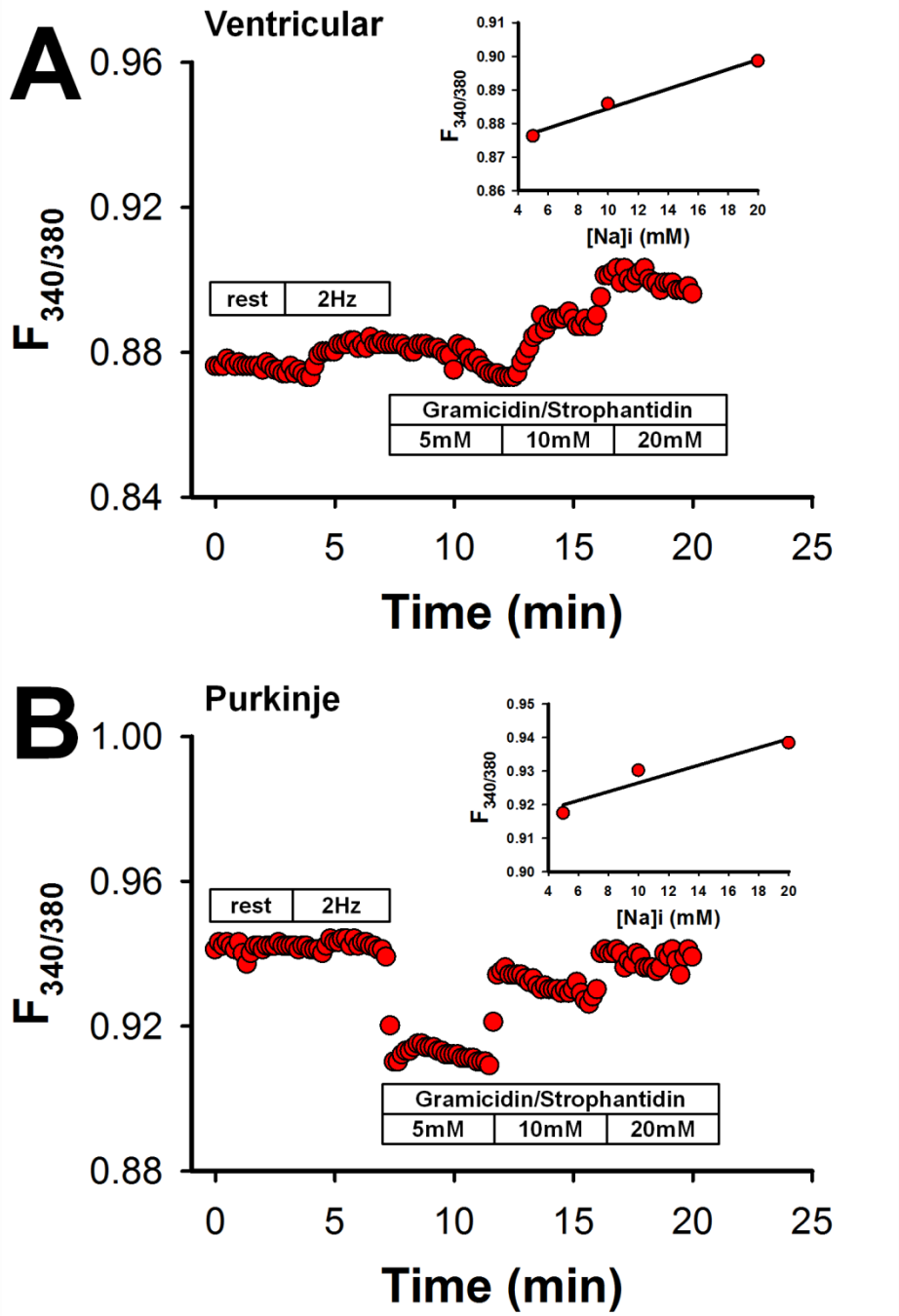

Supplement Fig. S8. Increased intracellular Na^+ in Purkinje cells compared to ventricular myocytes. Representative SFBI fluorescence recordings in (A) ventricular and (B) Purkinje cells at 37° C. Inset shows 3 point calibration performed at the end of each individual experiment after perfusion with gramicidin and strophantidin and three different increasing concentrations of Na^+.

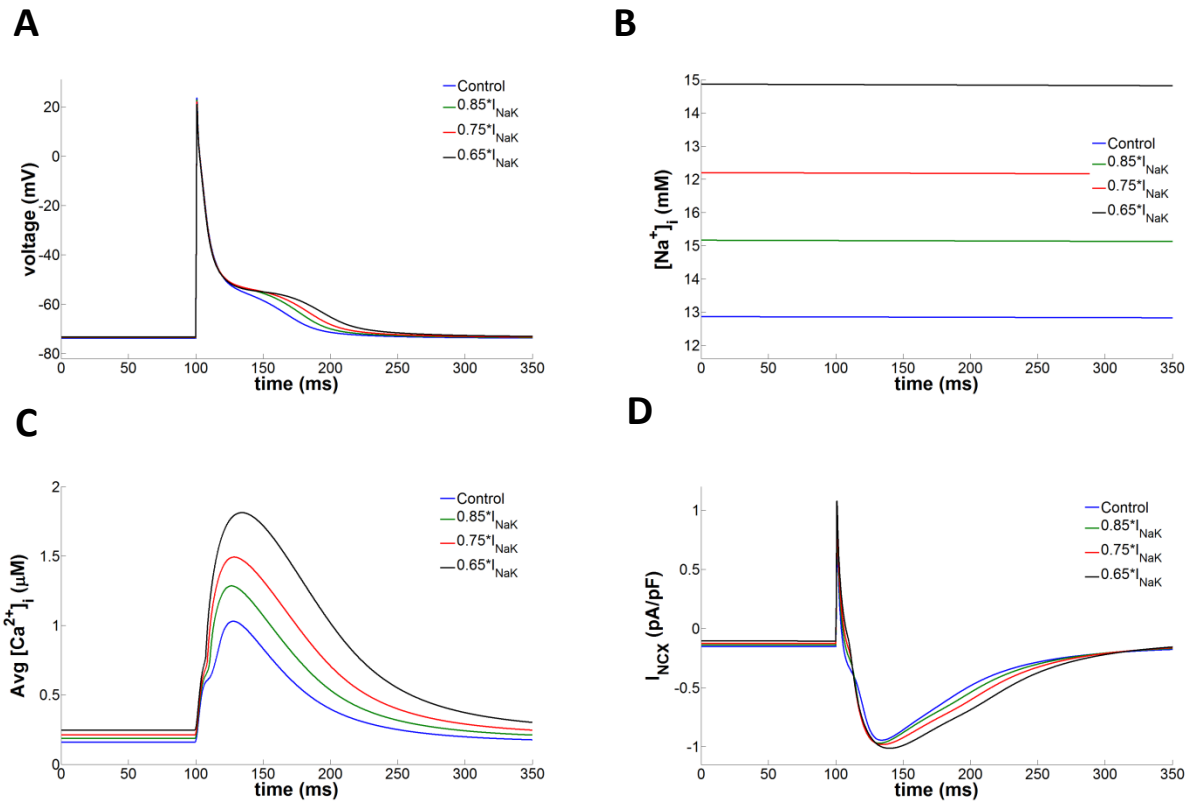

Supplemental Fig. S9. (A) Action Potentials in PC model for different scaling of I_{NaK} at 1Hz pacing. (B) Intracellular sodium concentration in PC obtained by scaling I_{NaK} at 1Hz (C) Intracellular average calcium concentrations in the model for different scaled I_{NaK} at 1Hz (D) I_{NCX} currents for different scaled I_{NaK} currents at pacing frequency of 1Hz.

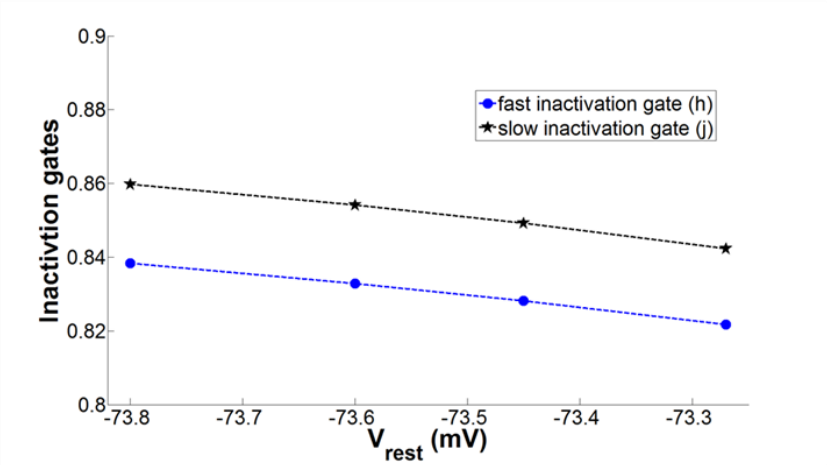

Supplemental Fig. S10. Insignificant alterations in the fast and slow inactivation gates (*h* and *j*, respectively) of I_{Na} at various resting membrane potentials resulted due to elevated levels of $[Na]_i$.

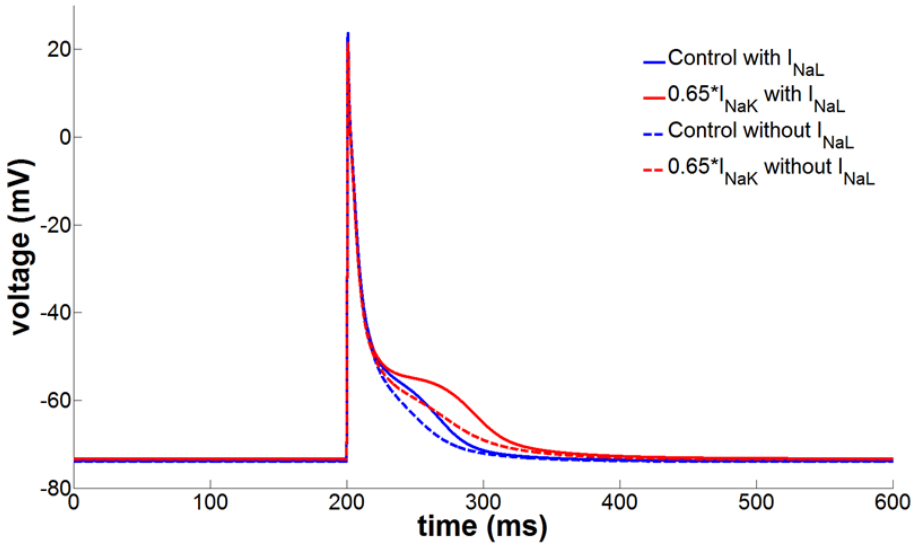

Supplemental Fig. S11. Action potentials in the PC model with I_{NaL} and without I_{NaL} for the control case and for one representative I_{NaK} value.

References:

1. Cerrone M, Colombi B, Santoro M, di Barletta MR, Scelsi M, Villani L, Napolitano C, Priori SG. Bidirectional ventricular tachycardia and fibrillation elicited in a knock-in mouse model carrier of a mutation in the cardiac ryanodine receptor. *Circ Res*. 2005;96:e77-82
2. Cerrone M, Noujaim SF, Tolkacheva EG, Talkachou A, O'Connell R, Berenfeld O, Anumonwo J, Pandit SV, Vikstrom K, Napolitano C, Priori SG, Jalife J. Arrhythmogenic mechanisms in a mouse model of catecholaminergic polymorphic ventricular tachycardia. *Circ Res*. 2007;101:1039-1048
3. Miquerol L, Meysen S, Mangoni M, Bois P, van Rijen HV, Abran P, Jongsma H, Nargeot J, Gros D. Architectural and functional asymmetry of the his-purkinje system of the murine heart. *Cardiovasc Res*. 2004;63:77-86
4. Fernandez-Velasco M, Rueda A, Rizzi N, Benitah JP, Colombi B, Napolitano C, Priori SG, Richard S, Gomez AM. Increased ca2+ sensitivity of the ryanodine receptor mutant ryr2r4496c underlies catecholaminergic polymorphic ventricular tachycardia. *Circ Res*. 2009;104:201-209, 212p following 209
5. Herron TJ, Milstein ML, Anumonwo J, Priori SG, Jalife J. Purkinje cell calcium dysregulation is the cellular mechanism that underlies catecholaminergic polymorphic ventricular tachycardia. *Heart Rhythm*. 2010;7:1122-1128
6. Lee P, Klos M, Bollensdorff C, Hou L, Ewart P, Kamp TJ, Zhang J, Bizy A, Guerrero-Serna G, Kohl P, Jalife J, Herron TJ. Simultaneous voltage and calcium mapping of genetically purified human induced pluripotent stem cell-derived cardiac myocyte monolayers. *Circ Res*. 2012;110:1556-1563
7. Noujaim SF, Pandit SV, Berenfeld O, Vikstrom K, Cerrone M, Mironov S, Zugermayr M, Lopatin AN, Jalife J. Up-regulation of the inward rectifier k+ current (i k1) in the mouse heart accelerates and stabilizes rotors. *J Physiol*. 2007;578:315-326
8. Anumonwo JM, Tallini YN, Vetter FJ, Jalife J. Action potential characteristics and arrhythmogenic properties of the cardiac conduction system of the murine heart. *Circ Res*. 2001;89:329-335
9. Vaidyanathan R, O'Connell RP, Deo M, Milstein ML, Furspan P, Herron TJ, Pandit SV, Musa H, Berenfeld O, Jalife J, Anumonwo JM. The ionic bases of the action potential in isolated mouse cardiac purkinje cell. *Heart Rhythm*. 2013;10:80-87
10. Cheng H, Song LS, Shirokova N, Gonzalez A, Lakatta EG, Rios E, Stern MD. Amplitude distribution of calcium sparks in confocal images: Theory and studies with an automatic detection method. *Biophys J*. 1999;76:606-617
11. Picht E, Zima AV, Blatter LA, Bers DM. Sparkmaster: Automated calcium spark analysis with imagej. *Am J Physiol Cell Physiol*. 2007;293:C1073-1081
12. Despa S, Islam MA, Weber CR, Pogwizd SM, Bers DM. Intracellular na(+) concentration is elevated in heart failure but na/k pump function is unchanged. *Circulation*. 2002;105:2543-2548
13. Li L, Niederer SA, Idigo W, Zhang YH, Swietach P, Casadei B, Smith NP. A mathematical model of the murine ventricular myocyte: A data-driven biophysically based approach applied to mice overexpressing the canine ncx isoform. *Am J Physiol Heart Circ Physiol*. 2010;299:H1045-1063
14. Stuyvers BD, Dun W, Matkovich S, Sorrentino V, Boyden PA, ter Keurs HE. Ca2+ sparks and waves in canine purkinje cells: A triple layered system of ca2+ activation. *Circ Res*. 2005;97:35-43
15. Crank J. *The mathematics of diffusion*. Oxford: Clarendon Press; 1975.
16. Korhonen T, Hanninen SL, Tavi P. Model of excitation-contraction coupling of rat neonatal ventricular myocytes. *Biophys J*. 2009;96:1189-1209
17. Sadiku M. *Numerical techniques in electromagnetics*. CRC Press; 2000.